



W&M ScholarWorks

Undergraduate Honors Theses


Theses, Dissertations, & Master Projects

5-2019

Construction of an Auger Microscope

Charles Soulen

Follow this and additional works at: <https://scholarworks.wm.edu/honorstheses>

 Part of the [Engineering Physics Commons](#), and the [Other Materials Science and Engineering Commons](#)

Recommended Citation

Soulen, Charles, "Construction of an Auger Microscope" (2019). *Undergraduate Honors Theses*. Paper 1359.

<https://scholarworks.wm.edu/honorstheses/1359>

This Honors Thesis is brought to you for free and open access by the Theses, Dissertations, & Master Projects at W&M ScholarWorks. It has been accepted for inclusion in Undergraduate Honors Theses by an authorized administrator of W&M ScholarWorks. For more information, please contact scholarworks@wm.edu.

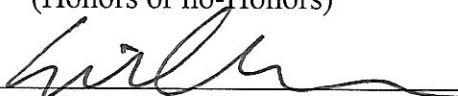
Construction of an Auger Microscope

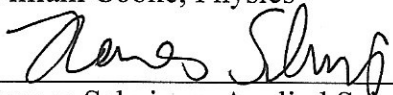
A thesis submitted in partial fulfillment of the requirement
for the degree of Bachelor of Science in Physics from
The College of William and Mary

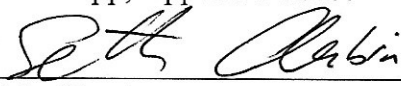
by

Charles Soulen

Accepted for Honors
(Honors or no-Honors)


William Cooke, Physics


Hannes Schniepp, Applied Science


Seth Aubin, Physics

Williamsburg, VA
May 2, 2019

Abstract

This thesis describes the design, adaptations and characterizations necessary to partially turn an Auger Electron Spectroscopy Instrument (AES) into an Auger Electron Microscope (AEM). The completed AEM will be able to scan and characterize materials over an area, unlike the AES which only took data from a single point. However, due to time constraints, this thesis only partially describes the creation of an AEM. We were able to show proof-of-concept, though, we were unable to run AEM on a material. We have also increased the theoretical accuracy of the instrument by replacing decades-old electronics with modern alternatives. Again, due to time constraints, we are currently unable to certify this, as we are limited by certain reoccurring errors in our data. Auger Microscopes are powerful tools in surface and deposition characterization. We intend to use the AEM to analyze deposition processes used in the creation of thin film solid state batteries and determine possible defects in the deposition process. To characterize the abilities of our instrument, we first replicated and compared our instrument against the spectrometer's current capabilities. Then we scanned the electron beam across a surface to show that we can create a one dimensional map of our Cylindrical Mirror analyzer's focal point. While we have not successfully shown Auger Microscopy with this instrument, we have left this project with the necessary tools to do so.

1 Introduction

Electron spectroscopy has become a common form of chemical and surface analysis. In general, there are two main types of electron spectroscopy; Auger Electron Spectroscopy(AES), in which Auger electrons are produced via an electron beam and energy analyzed [1], and X-ray Photoelectron Spectroscopy (XPS), in which photoelectrons are produced via an X-ray beam and are energy analyzed [1]. These techniques are often combined into a single instrument, known as a Combined XPS and AES Spectrometer [3].

This honors thesis describes efforts towards converting an Auger Spectrometer, which only allows for AES analysis at a single point, to an Auger Microscope, which allows for AES analysis over an area. This required the replacement of legacy electronics and software with modern alternatives. We accomplished this task in two

parts. First, we rebuilt the Spectrometer with modern hardware and software and improved on the signal to noise ratio of the instrument, when compared to the legacy components. Next, we created the Auger Microscope by scanning the electron beam over an area. Unfortunately, due to time constraints, we were unable to complete the Auger Microscope. However, this thesis does leave the overarching project in a prime position to complete the Microscope. This thesis will refer to the legacy equipment as the Legacy Electronics system(LE system) and the modern alternative as the Microprocessor Controlled system(MPC system).

With regards to a larger project, the Auger Microscope will be used in the characterization of material deposition techniques used in the creation of solid-state batteries. We will typically run the MPC system using a 2 *keV* electron beam, allowing us to analyze only the first atomic layer, since Auger electrons scatter quickly within materials. Thus, the only useful signal comes from the top layer of atoms. More information on this process will be provided later in this paper. Moreover, we can estimate how small of an object we will be able to image based on a secondary surface microscopy option provided on the LE system called Stage Current Microscopy. Using this option, we raster the electron beam and measure the current collected by the stage from the electron beam. We then feed the collected stage current into a CRT TV, producing an image of a portion of the stage. Objects placed on the stage will change the amount of collected stage current, producing images on the TV. This technique allows us to image objects on the order of 100 μm . Therefore, we estimate that we will be able to use AEM to image objects on a similar scale.

2 Theory and the AES Instrument

2.1 Auger Electron Spectroscopy

2.1.1 X-Ray Notation

In Auger Electron Spectroscopy, we primarily use X-ray notation to denote the electron transitions occurring during AES. X-ray notation defines electron orbitals with a letter and a subscript numeral. The letter, starting with K and proceeding upwards, represents the electron shell, or n quantum number. A K shell electron would therefore be in the first, or $n = 1$, shell and an M shell electron is located in the third, or $n = 3$, shell. The subscript numeral represents the location of the electron within the shell based on the subshell and absolute value of the total angular momentum quantum number, j . Therefore, since a $1s^2$ electron can only have $j = \pm 1/2$, it is denoted by a I. The p subshell, on the other hand, can have angular momentum $j = \pm 1/2, \pm 3/2$ and is therefore represented by the subscript values II and III. Note that the subscript values increase with both the subshell and the value of j . Combining the letter and subscript notations in an example, the x-ray notation of a valence oxygen electron ($1s^2 2s^2 2p^4$) with $j = \pm 1/2$ would therefore be L_{II} in x-ray notation.

2.1.2 Creating Auger Electrons

In order to characterize a material, Auger Spectroscopy requires the capture and energy analysis of Auger electrons. To produce these electrons, we first bombard the sample with a high energy electron beam. When an incoming electron collides with a core electron, and exceeds its binding energy, the core electron may be ejected, leaving the atom in an ionized, excited state. Two of the remaining electrons collide, sending one to fill the lower shell, while the other is ejected from the atom with the remaining energy. The ejected electron is called the Auger electron. Its kinetic energy

is characteristic of the parent atom and, occasionally, its chemical environment. This allows for elemental identification based on the energy of the Auger electron [1]. A diagram of this process is shown in Figure 1

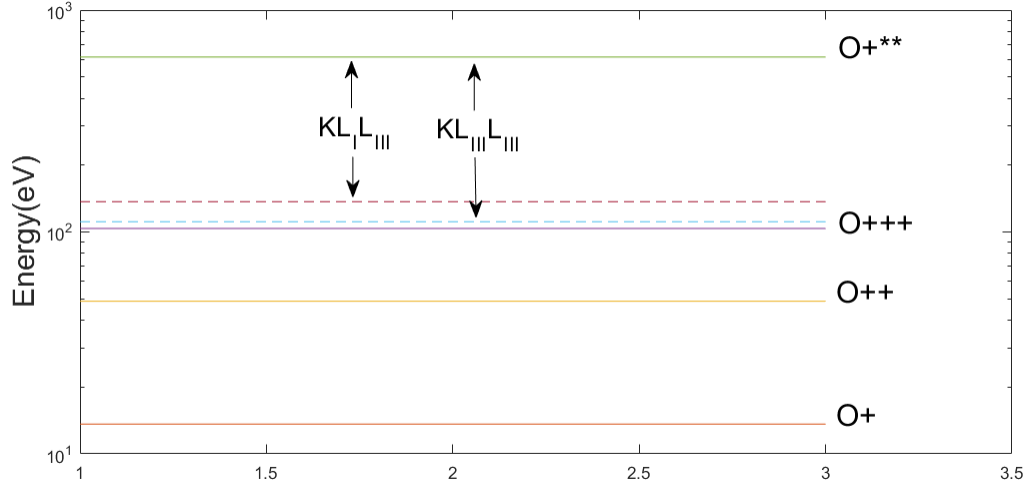


Figure 1: An energy level diagram for the $KL_I L_{III}$ and $KL_{III} L_{III}$ Auger transitions. Note that these transitions occur after the oxygen atom has entered a doubly excited, ionized state. One of the excited electrons drops to a lower energy state (represented by the dashed lines) and forces a different electron out of the atom. This electron has an energy represented by the $KL_I L_{III}$ and $KL_{III} L_{III}$ arrows shown in this diagram.

We denote which transitions occur by using X-ray notation. We use three letters in series to denote the initially emitted electron, the relaxing electron, and the Auger electron, respectively. Thus, if a K shell electron is initially ionized, an L_I electron relaxes, and an L_{II} electron is emitted as the Auger electron, we denote this process as $KL_I L_{II}$. Auger electrons emitted from this process would have energy equal to

$$E_{Auger} = E_K - E_{L_I} - E_{L_{II}} - \phi \quad (1)$$

Where E_K , E_{L_I} , and $E_{L_{II}}$ are the binding energies of their respective electrons and ϕ is the work function of the material. This equation can be generalized to apply

to any three part Auger process. Values for the various energy levels can be found in compendiums online, or in Auger spectroscopy books such as *The Handbook of Auger Electron Spectroscopy*, which we used in this thesis. A transition diagram of the process is shown in Figure 2.

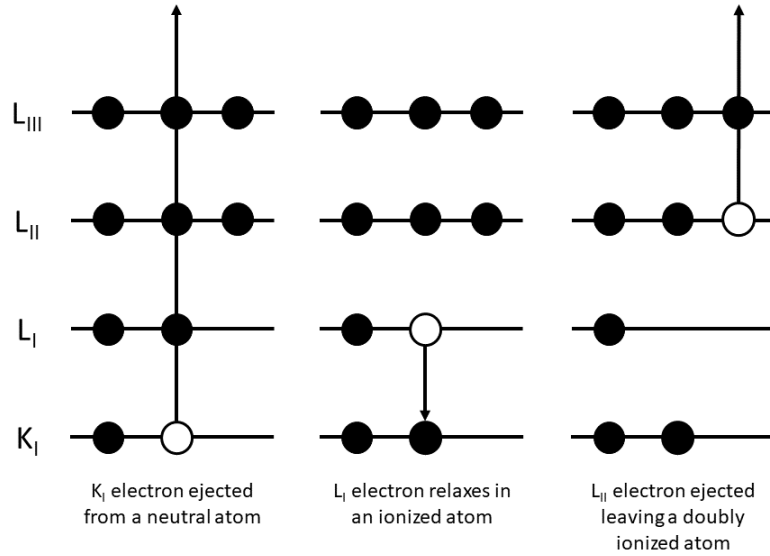


Figure 2: Transition diagram of a $KL_I L_{II}$ Auger transition. Black circles represent electrons and white circles represent holes left by transitioning electrons

2.1.3 Analysis of Auger Electrons

The result of the creation of Auger electrons is a notable increase in the number of detected electrons as we scan our energy analyzer near an Auger energy, E_{Auger} . This spike in electrons is known as an Auger peak, examples of which can be seen in Figure 3. Historically, we would take the derivative of the spectrum to show the Auger peaks more clearly and to remove background noise. However, in this thesis, we generally use the Auger spectrum for analysis. These plots are known as the Auger spectrum and the derivative spectrum, respectively. Most elements allow for multiple electron transition, which produce Auger electrons with a variety

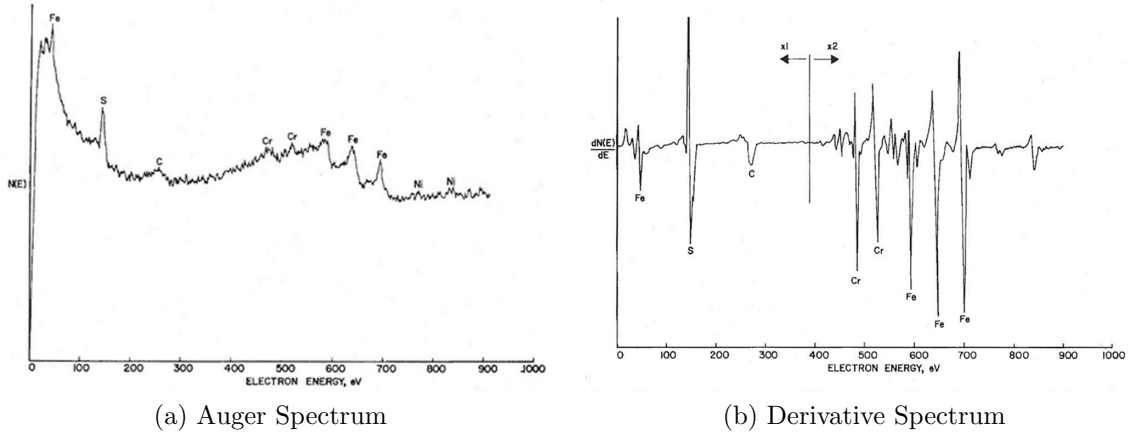


Figure 3: An Example of an Auger spectrum, left, and its corresponding derivative spectrum, right. Adapted from PW Palmberg (1974), Combined ESCA and Auger Spectrometer. *Journal of Vacuum Science and Technology*, Vol 12, No. 1. Pg. 379.[3]

of energies. Therefore, we see multiple peaks per element, each with its own unique electron transition series and Auger energy. For example, iron has three major Auger peaks between 500 eV and 750 eV . These three peaks can be seen in Figure 3.

2.2 The Auger Electron Instrument

The first step in an AES instrument is the production of the Auger electrons themselves. Both the LE and the MPC systems use a 2 keV electron beam to produce Auger electrons. We have the option to increase or decrease the electron energy, however, we use 2 keV as a comparable energy to the maximum detectable energy of our Cylindrical Mirror Analyzer(CMA), as discussed in the next paragraph. Increasing the electron beam energy would allow us to access higher energy Auger transitions necessary to remove the core electrons from heavier elements. However, the energy of these Auger electrons may exceed the maximum measurable energy of our current CMA. Without the need to access Auger transitions above 2 keV , we have decided to keep the electron beam energy at 2 keV .

For our AES instrument to function, it needs to energy-analyze the Auger electron. To do this, our instrument employs a Cylindrical Mirror Analyzer. The CMA energy selects Auger electrons scattered into a solid angle of $42.3 \pm 6^\circ$, as determined by the CMA [3]. The electrons which enter this solid angle are deflected by a cylindrical voltage grid and pass through an aperture to reduce the bandwidth of the selected energy. They are deflected a second time by the same voltage grid and pass into the electron multiplier, which amplifies the signal so that it can be read. Thus, the number of detected electrons within a certain energy bandwidth corresponds to the voltage output of the electron multiplier. The inner cylinder of the CMA is held at $0V$. A diagram of this process is shown in Figure 4.

The maximum detectable energy of our CMA is constrained by the high voltage used to power the voltage grids. For both the LE and the MCP systems, we use 2 kV high voltage, which limits the detectable Auger electron energy to 2 keV . We could increase this value by replacing the high voltage power supply, however, for this project, we have decided to leave the high voltage supply unchanged. The resolution of our CMA is calculated as $R = \frac{\Delta E}{E} = 0.6\%$ [3]. Palmberg et. al. estimates this value based on the size of the aperture located in the center of the CMA, which has a radius of about 2 mm .

To read the voltage provided by the CMA, the LE system uses a Voltage to Frequency converter (VFC), which has a maximum frequency of 1 MHz and a minimum frequency of 2 kHz . This results in a dynamic range of $\frac{1\text{ MHz}}{2\text{ kHz}} = 500$. The VFC reads the voltage output of the CMA with respect to a 2 kV ground while also shielding the output from the high voltage to a maximum of 5 kV . The frequency output of the VFC is linearly proportional to the voltage input, with a bandwidth of 150 Hz . Thus, the maximum theoretical precision of the LE system is $\frac{150\text{ Hz}}{1\text{ MHz}} = .00015$ or

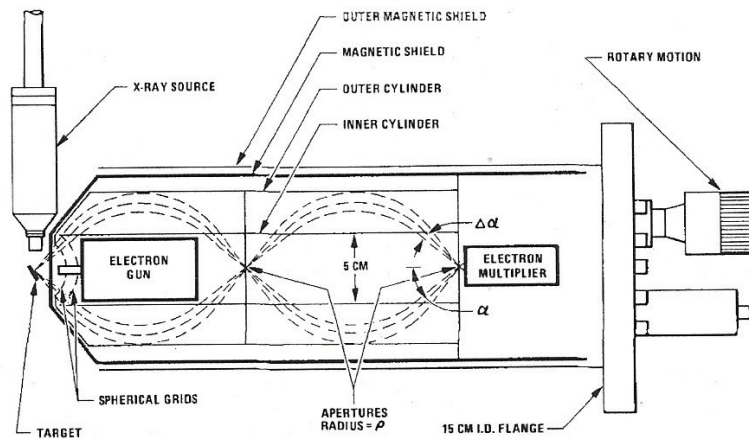


Figure 4: An example of an Auger instrument using a CMA. Adapted from PW Palmberg (1974), Combined ESCA and Auger Spectrometer. *Journal of Vacuum Science and Technology*, Vol 12, No. 1. Pg. 379. [3]

about a part in 7,000. This frequency passes through a transformer, which insulates the high voltage, and into a frequency counter. This information is then transferred to a computer and plotted, creating an Auger spectrum of electron intensity as a function of electron energy[2].

At the beginning of this project, the LE AES instrument functioned as described above. It also contained several other functions, such as X-ray spectroscopy, but these functions are not the main subject of this thesis and will not be commented on. While the instrument functioned properly, there were several areas where we believed we could improve on the instrument.

2.3 Motivation

Primarily, we wanted to adapt the instrument to scan over an area rather than at a single point. The adaptation of the instrument to include scanning, known as microscopy, would allow for material characterization over an area, making the instrument far more useful. Secondly, we believed that we could improve the accuracy

of the instrument. Many parts of the instrument, both hardware and software, were well over a two decades old. By replacing these with newer, more accurate electronic chips, we believed we could improve the accuracy of the instrument. In addition to this, much of the LE system's software was inaccessible. This prevented us from properly understanding the analytic techniques the software was using. By writing our own analytic software, we are able to completely understand the techniques used, as well as allowing for the possibility of improvement and customization in the future.

3 Constructing The Auger Electron Microscope

To create the Auger Electron Microscope, we split our project into two parts. First, we would replicate the AES instrument using modern electronics and new software. Second, we would create the Microscope by scanning the electron beam across a surface to create a real-time map of the sample.

3.1 Recreating the AES Instrument

The first step in recreating the AES instrument was to replace the Voltage to Frequency Converter. We did this in multiple steps. First, we needed to read a voltage with respect to a variable ground. To do this, we used a ADS1115 16 bit Analogue to Digital Converter(ADC) connected to an Mbed microcontroller using an I^2C communications line. The ADS1115 has a theoretical accuracy of a part in 2^{16} , or about 65,000 and a theoretical data collection rate of about 1 kHz . Compared to the VFC from the LE system, this is a improvement on the dynamic range by a factor of about 10. By averaging over many data points, we are able to collect more accurate data and provide a standard deviation of the average. The LE system does not provide either of these two data sets. We chose the Mbed microcontroller as we had already learned how to connect the Mbed to MatLab during a previous project

and planned to create a similar connection to create plots and run data analytics.

Next, we needed to be able to read voltages with respect to a 2 kV ground. At such high voltages, we needed to insulate our ADC from our Mbed. We used a CPC5902 opto-isolator to insulate the I^2C lines and a REM1-3.33.3S DC-DC converter to insulate the 3.3 V line used to power the ADS1115. We also included a 1 $M\Omega$ resistor and dual diodes to protect the delicate ADS1115 from possible voltage surges.

We decided to set the data rate of the ADS1115 to its maximum in order to obtain as much raw data as possible. To aid in the integration of the signal, we included a 2 μF capacitor in parallel with our 1 $M\Omega$ resistor. This allowed us to integrate the signal over a time period while gathering as much raw data as possible. To avoid retaining too much of the previous measurement, or conversion, we chose a capacitor which, in parallel with a 1 $M\Omega$ resistor, results in a low pass filter with 3dB point of 1 ms . Thus, the majority of the previous conversion will have dissipated by the time a new conversion is completed. In this way, we are able to integrate our signal over a time period while also gathering copious amounts of raw data.

Thus, we were able to read voltages with respect to a 2 kV ground and pass them to an Mbed without damaging it. The complete diagram of this circuit is shown in Figure 5. On the top left of this diagram, we can see dual diodes along with a 2 μF capacitor in parallel with a 1 $M\Omega$ resistor. Along the edge of this corner, we have the signal input, the high voltage input and the high voltage output, protected by a 220 $k\Omega$ resistor. All of these connections link to MHV wires, which run to the electron multiplier(signal in and HV out) or the high voltage power supply (HV in). In the bottom left corner of the diagram is the ADS1115. We have connected the

2 kV ground to the A0 pin and the signal input to the A1 pin. The I^2C lines (SDA and SCL) connect to the optoisolator, and the VCC and ground lines connect to the DC-DC converter. In the top right of the box is the DC-DC converter, which accepts 5 V on the right and outputs 3.3 V with respect to the 2 kV ground on the left. Below the DC-DC converter is the optoisolator. This isolates the high voltage I^2C lines from the low voltage I^2C lines, allowing us to communicate with a serial port using I^2C . Finally, on the right of the diagram is the low voltage output, which runs through a PS2 wire to the Mbed.

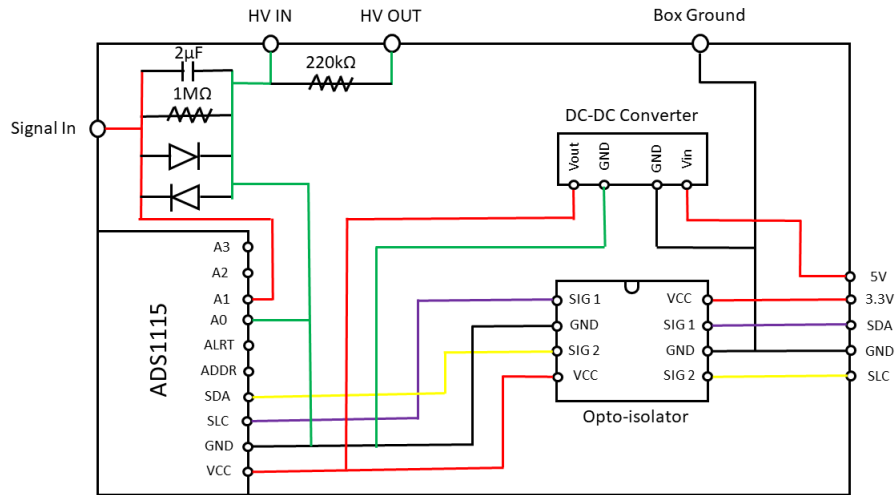


Figure 5: The circuit diagram of the ADC. High voltage electronics appear on the left of the figure, and insulating electronics appear on the right. The wire colors in the figure match the colors used in the physical circuit.

3.2 Software

The creation of the software needed to run the ADC was fairly straight forward. The ASD1115 comes with multiple features and modes, which allows for flexibility in usage. For our purposes, we use continuous conversion mode, which automatically begins integrating the voltage input as soon as the previous conversion has been

completed. The ADS1115 completes conversions at a rate equal to the data rate, which, using our settings, was 860 samples per second, or one conversion every 1.2 *ms*. The completed conversions are then placed in the conversion register, until they are read or overwritten by the next conversion. We poll the ADS1115 every 1.4 *ms*, which recalls the last completed conversion. Although we do occasionally miss a conversion, this occurs infrequently enough that we consider it insubstantial. Using the programmable gain amplifier built into the ADS1115, we set the maximum measurable voltage to ± 0.256 V, increasing the precision of the ADS1115 at low voltages. This is ideal for our purposes as the voltages we are measuring are less than ± 0.256 V.

For each data point, we average over 142 conversions, or once every 200 *ms*. To do this, we collect 142 conversions and store them in a vector on the Mbed. Then, we export the conversions to MatLab and take the average and the standard deviation of the data set. Next, we plot mean and the standard deviation while preserving the raw conversion data in a separate matrix. All of these values are user-defined through MatLab using Remote Procedural Commands (RPCs). Thus, if the user wants to average over 100 conversions rather than 142, they only have to change one variable in the MatLab script. This allows for complete customization according to the user's needs.

3.3 Replacing the Voltage to Frequency Converter

Now that we had a working ADC, we integrated it into the AES instrument. By simply replacing the Voltage to Frequency Converter with the new ADC, we were able to partially bypass the LE system's data collection software. Now, the LE system's software stepped the CMA voltage as the MPC system measured the voltage out of the electron multiplier. Since the VFC is physically separate from the AES Instrument, we were able to switch between the new ADC and the VFC at will. This

has proved useful in the characterization of the new ADC.

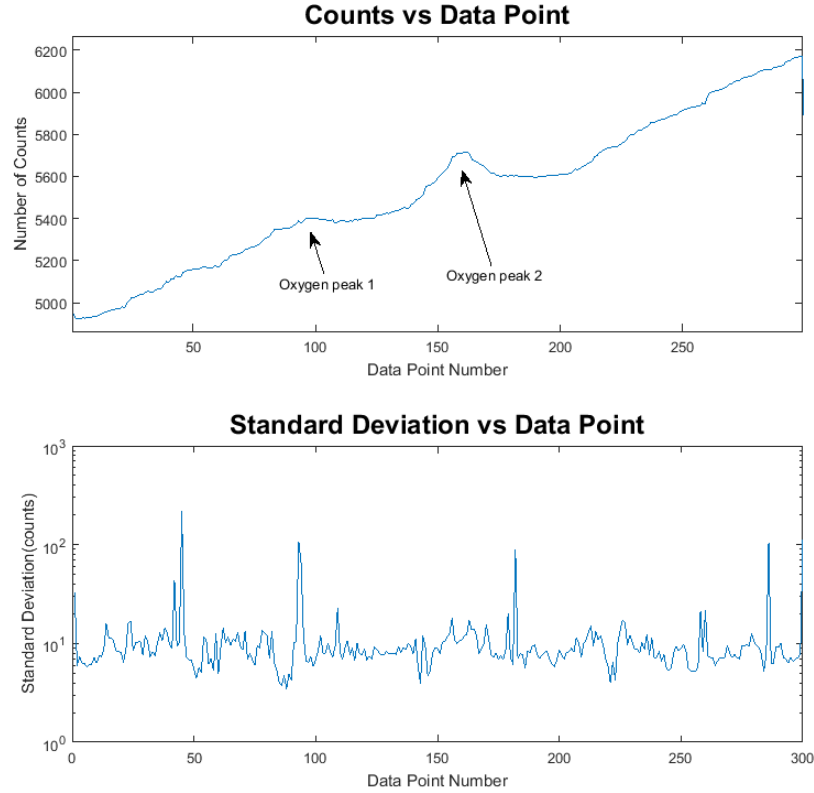


Figure 6: Representative data, taken January 15th, 2019 of the Auger Oxygen peak. There are clearly two oxygen peaks present, and the standard deviation is low, except for the occasional glitch. Note that the x-axis is measured by data point number. This is because, when this data was taken, we had not yet included the conversion to voltage. In this graph, the selected Auger electron energies range from 450 eV to 550 eV.

3.4 Replacing the CMA Voltage Stepper

Once we were able to successfully collect data using the ADC, we wanted to replace the Digital to Analogue(DAC) converter used to step the voltage on the CMA. This would allow us to consolidate the data collection system onto a single computer. We decided to use a AD5761 16-bit DAC set to provide a 0 – 10V range. The output of the AD5761 is fed into an amplifier with a gain of 200 and into the outer cylinder

of the CMA, while the inner cylinder is held at 0V. This allows us to control which electron energies are selected by the CMA. Finally, we connected the AD5761 to our Mbed using an SPI serial interface, and adapted our Mbed and MatLab codes to step the DAC voltage while taking data on the ADC.

Using this system, we were able to optimize the electron beam position and power, and the CMA high voltage. Thus, we were able to start collecting data of the Auger spectrum. A representative plot of this is shown in Figure 6. Note that the standard deviation of the data set is very low, apart from occasional glitches, which will be discussed in the next section.

4 Characterizing the Auger Spectrometer

The next step in our process was to understand how well our spectrometer worked and to identify any sources of error and eliminate them. We especially wanted to prove that the signal to noise ratio (SNR) of our new system outmatched the old system.

4.1 Signal to Noise Ratio

In order to directly compare the LE system to the MPC system, we calculated the signal to noise ratio. To do this, we set the CMA to scan for the elastically scattered electrons, and collected data for 7.5 minutes on each of the two systems. Then, we took the average and standard deviation of each data set. The SNR is calculated as $SNR = \frac{\textit{average}}{\textit{standard deviation}}$. Thus, we found the SNR of the LE system to be 371.9 and the SNR of the MPC system to be 4246.3. We have, therefore, improved on the SNR of the LE system by about a factor of 10.

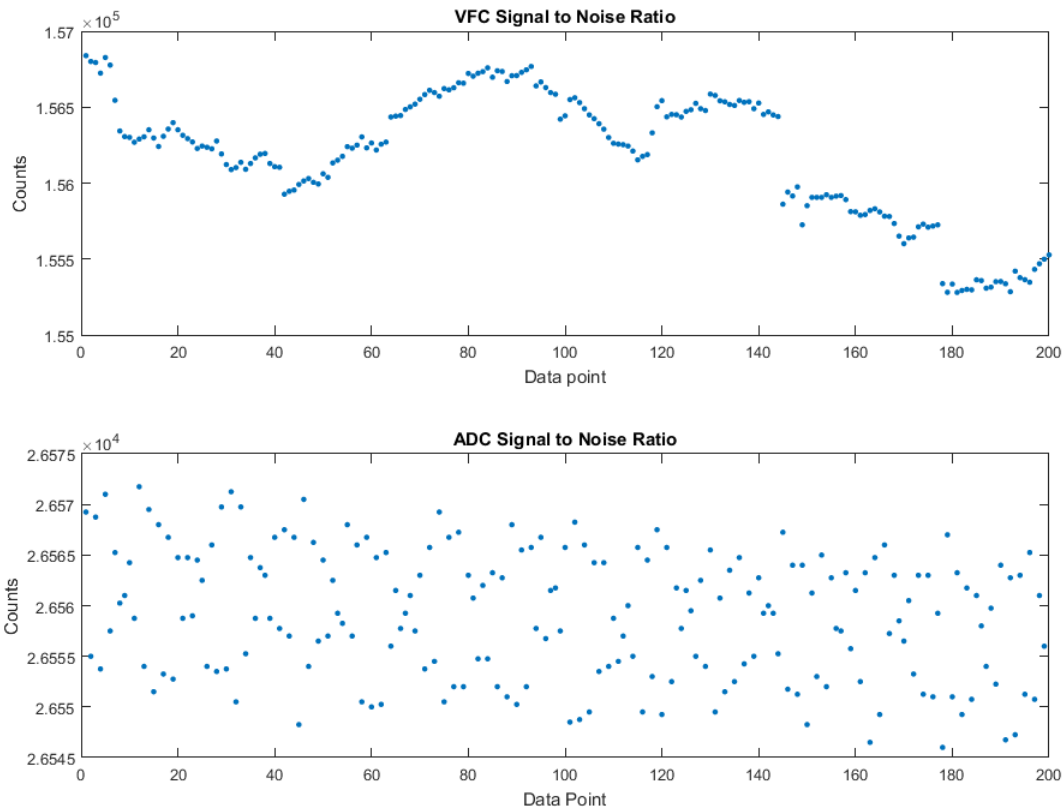


Figure 7: A signal to noise ratio test showing the elastically scattered electrons. Note that the ADC has randomly distributed data points, while the VFC has a clear structure. This suggests that the ADC has less systematic offsets than the ADC.

4.2 Errors in the System

We have noticed two types of glitches that appear in our data. First, we see occasional, but dramatic, jumps in the signal size for a single data point. An example of this is shown in Figure 8. Upon further inspection, we discovered that, within the set of conversions averaged to create these data points, only a single conversion would have an erroneous value. Figure 9 shows this for the point error occurring in Figure 8. Thus, we conclude that these are not real errors, but are errors occurring during the transfer process from the ADC to the Mbed, or from the Mbed to MatLab. Theoretically, we could write a Matlab script to filter out these errors, although we

have not done so yet as these errors are obvious and easy to fix manually.

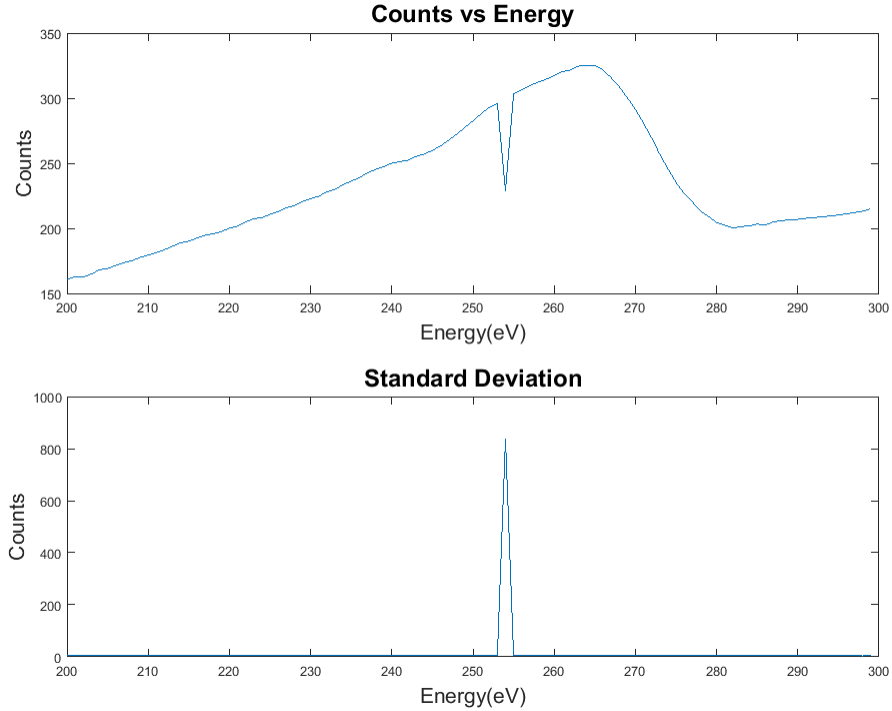


Figure 8: An example of a point error, taken February 20th, 2019 of the Auger carbon peak. Note that this error results from a single point within the mean suddenly having a large or small value. This phenomenon is shown again in Figure 9

The second type of error we have noticed occurs when an entire section of data either jumps or falls dramatically, while keeping the same general trend. An example of this is shown in Figure 10. Following the same process we used for the point errors, we plotted the set of conversions over which we saw a jump error. An example of this is shown in Figure 11. While investigating this error, we measured the electron beam current (by measuring the stage current), the voltage on the x-y deflection grids, and the high voltage running to the electron multiplier. We did not find any conclusive evidence that any of these variables were the source of the jump errors.

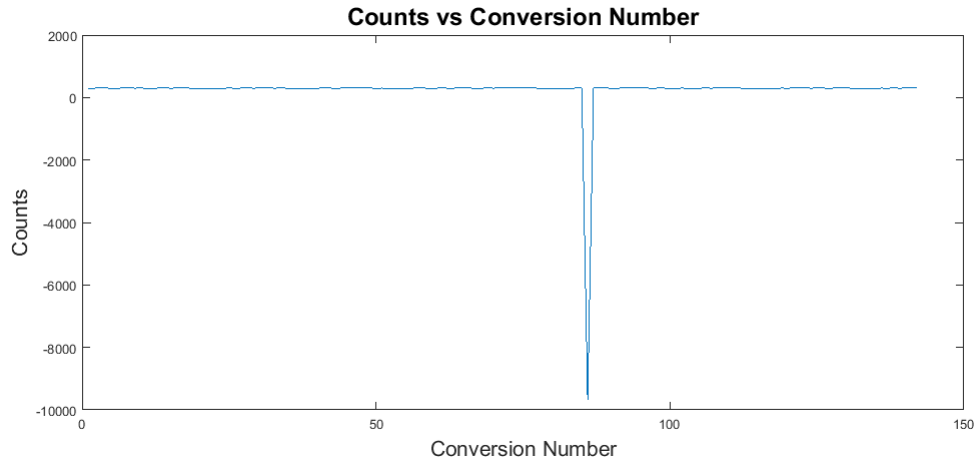


Figure 9: A plot of the conversions averaged to create point 254 eV in Figure 8. Note that the majority of the error is caused by a single conversion within the mean. We believe this is due to an error occurring during data transfer.

Finally, while attempting to determine the cause of these errors, we measured the signal size while alternating the energies selected by the CMA to either be on or above the elastically scattered electron peak. This would give us signals on the order of 20,000 counts or near 0 counts depending on whether we are on or above the elastic electron peak, respectively. This allowed us to measure the response time of our system, which we found to be 15 conversions, or 20 ms . The resultant plot is shown in Figure 12. Compared to the response time of the jump error, which we measured to be 17 conversions, or 24 ms , we have determined that this is the same response time. Thus, these error are real and are due to problems in our electronics.

Although we were unable to correct these errors physically, we did discover that we could remove them digitally. By subtracting the jump height off of the affected section of data, we could produce a single, continuous plot of our data. Figure 13 shows the data from Figure 10 with the jump errors removed in this manner. Note that the standard deviation of the corrected data has not changed. This is because we have only added or subtracted a constant as necessary. Thus, the standard deviation

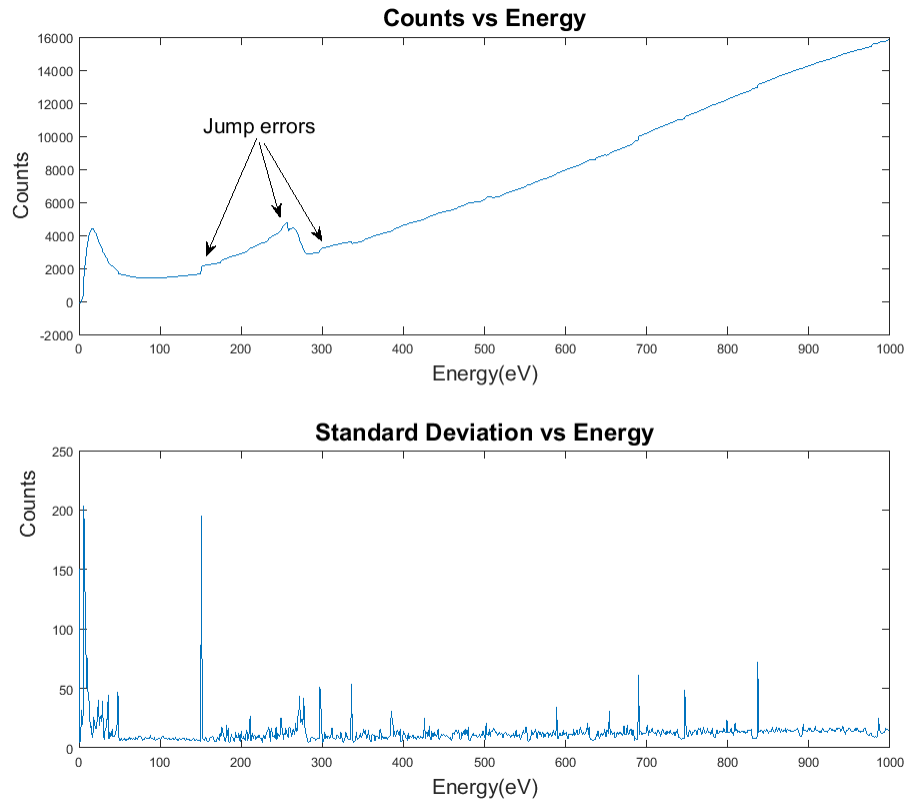


Figure 10: An example of a jump error, taken February 14th, 2019 of the full Auger Scan. Note that the jump errors appear as though a section of the code suddenly shifted either upwards or downwards

is unaffected.

This is not, however, a permanent fix. While investigating these jump errors, we noticed that they also started occurring with the LE system, where they had previously been undetected. Thus, we concluded that these error are real, although we are still unsure of the source. The jump errors are the major limiting factor of this project. Finding and correcting these errors will be the first improvement of this system after this thesis has been complete. However, we decided to move on to Auger Microscopy with the theory that AEM would provide more tools with which we could investigate the jump errors.

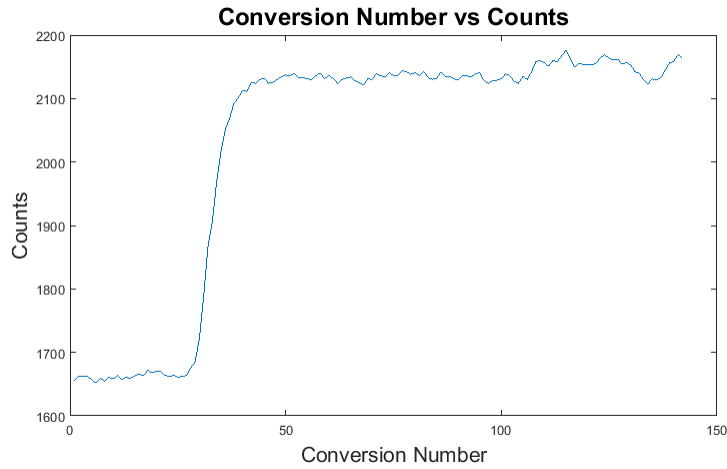


Figure 11: An example of a jump error occurring within the data set of point $152eV$ on Figure 10. This set shows how the signal size can suddenly jump in values. In a normal conversion set, this plot would be relatively constant, with a standard deviation of 10 to 20 counts.

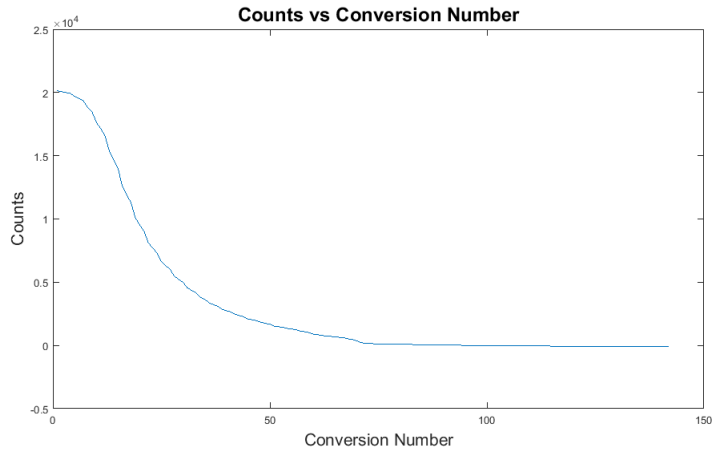


Figure 12: An example of the response time of the MPC system found by alternating between measuring energies on the elastic peak, and off of the elastic peak. Note that the response time is large compared to the jump error data set.

5 Auger Microscopy

With the spectrometer mostly working, we moved on to Auger Microscopy. This would require some hardware and software adaptations. Unfortunately, due to time constraints, we were unable to complete this conversion. First, we began with one

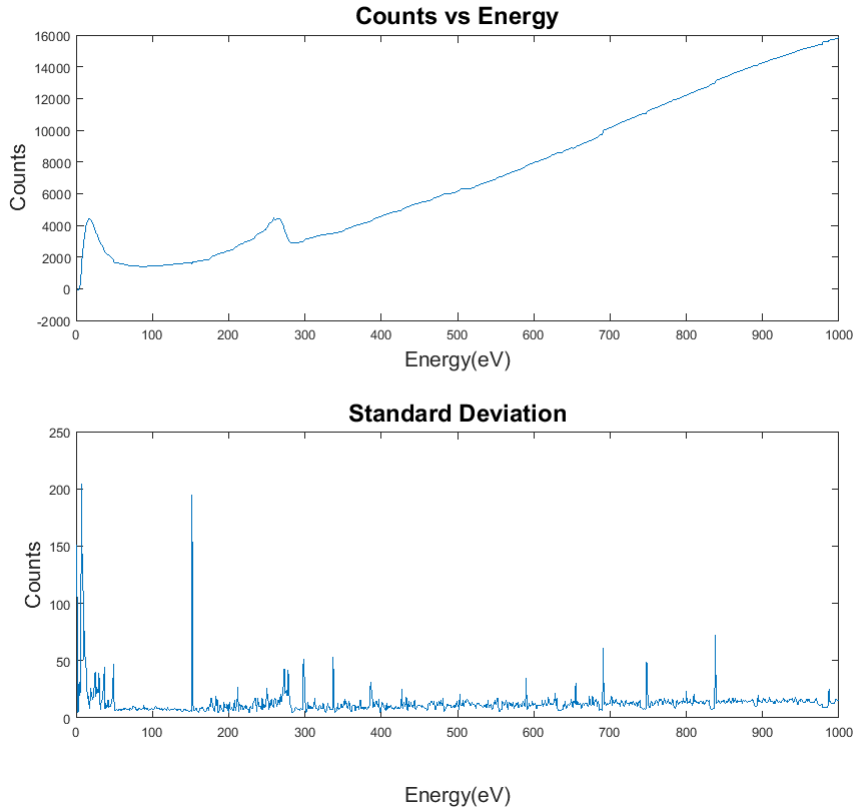


Figure 13: An example of the removal of jump errors. This plot shows Figure 10 with the two major jump errors removed. Note that the standard deviation of the data does not change. This is because we have only added or subtracted values as necessary, leaving the standard deviation unaffected.

dimensional Auger Microscopy as a proof of concept.

5.1 One Dimensional Auger Microscopy

The LE system is capable of steering the electron beam using a set of four voltage grids (two in x , two in y), which deflected the beam based on two dial settings on the electron beam control box. Each set of grids applies an equal and opposite voltage to the electron beam, in order to keep the mean voltage at 0 V , preventing the acceleration or deceleration of the electron beam. Thus, if 10 V are supplied to the top y -axis deflection grid, the bottom y -axis deflection grid would receive -10 V . We

used these grids to sweep the electron beam for AEM. To test this, we believed that we could deflect the electron beam in and out of the CMA's focal point, which would result in a change in signal size. To prove this concept, we set the CMA to scan for the elastically scattered electrons, which provides a relatively constant signal. Then, using the deflection dials, we scanned the electron beam in and out of the CMA's focal point. As expected, the signal size dropped noticeably outside of the focal point.

Next, we needed to take control of the deflection grids and replicate the previous result. Using the deflection dials, we determined that y -axis deflection would provide the greatest change in signal, about 2%, within the $\pm 10 V$ range of a second AD5761 DAC. Next, we connected our DAC to the y -axis deflection grids by removing the lead connecting the deflection control box to the AES instrument, and inserting our own lines into the appropriate ports. We grounded the x -axis grid control lines to each other. Finally, using newly written code, we set the CMA to look for elastically scattered electrons while scanning in and out of the CMA focal point. This test proved successful, showing the signal strength of the elastically scattered electrons falling as we moved in and out of the CMA focal point. An example of one of these scans is shown in Figure 14, where the y -deflection grid steps its voltage by $0.1 V$ every $200 ms$. The deflection grid runs between $0 V$, represented by the peaks, and $10 V$ represented by the troughs. Note that there are reoccurring spikes in the standard deviation about halfway through each individual scan. This is due to the signal size changing quickly, as seen at the corresponding points on the "Counts vs Voltage" plot. We could remove these spikes by reducing the size of the voltage step size or by increase the time over which we average our conversions.

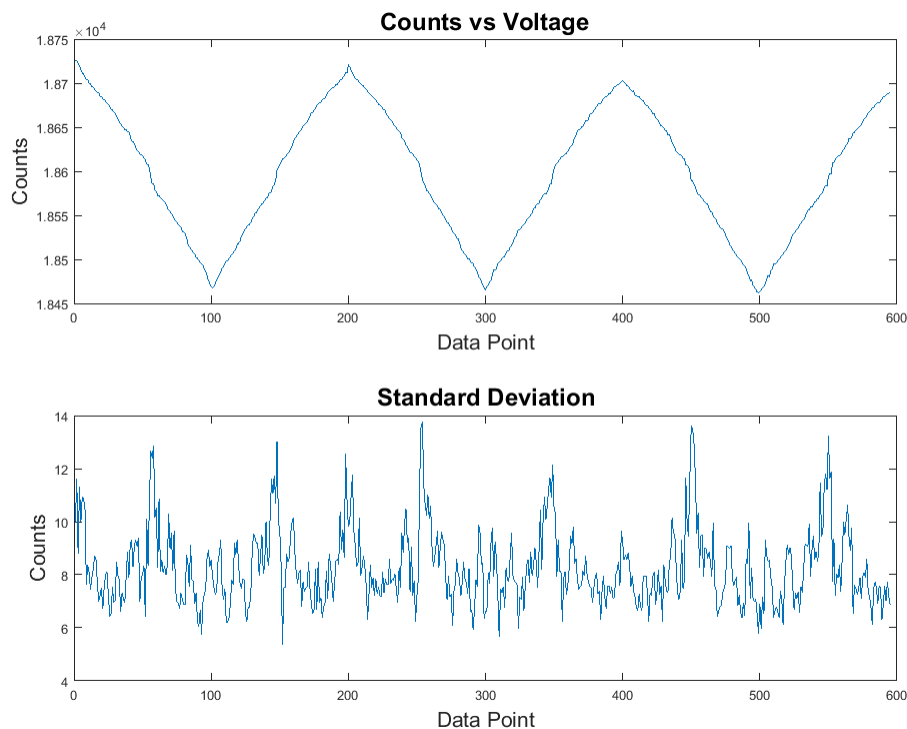


Figure 14: An example of a one dimensional Auger Microscopy scan, taken March 23rd, 2019 of the elastically scatter electrons while scanning the electron beam in and out of the CMA’s focal point. Note that the spikes in the standard deviation are caused by quick changes in the signal size, as seen on the ”Counts vs Voltage” plot.

6 Conclusion

Auger Electron Microscopy will prove to be a powerful tool in the characterization of the deposition processes we use in the creation of solid state batteries. In this thesis, we have created a useful proof-of-concept machine. Due to the time lost investigating the jump errors, we were unable to prove that the MPC system is capable of Auger Electron Microscopy. However, we have gathered all of the necessary components for a Auger Microscope. First, we have shown that we can successfully conduct Auger Electron Spectroscopy, although we have to filter out the occasional error. Second, we have shown that we are able to raster the electron beam across

a surface by taking control of the x-y deflection grids within the instrument. Thus, although we have not successfully completed an AEM scan, we have left this project with the necessary tools to do so.

The future of this project after this thesis lies in two areas. First, we need complete the Auger Microscope using the MPC system. Thanks to the work of this thesis, finishing the Auger Microscope should be a relatively simple task. Secondly, we need to further investigate the jump errors and determine their cause and how to fix them. This will likely require a detailed investigation into the electron multiplier and the CMA as these are currently the strongest suspects for the cause of these errors.

References

- [1] Chung, Y. (2001). *Practical Guide to Surface Science and Spectroscopy*. San Diego: Academic Press. Retrieved from <https://proxy.wm.edu/login?url=http://search.ebscohost.com/login.aspx?direct=trueAuthType=cookie,ip,url,shibdb=nlebkAN=195194site=ehost-livescope=site>
- [2] Watson, D. G., Larson, P. E., Paul, D. F. and Negri, R. E. (2012), High Energy Resolution Auger Spectroscopy on a CMA Instrument. *Surf. Interface Anal.*, 44: 121-125. doi:10.1002/sia.3782
- [3] PW Palmberg (1974), Combined ESCA and Auger Spectrometer. *Journal of Vacuum Science and Technology*, Vol 12, No. 1. Pg. 379
- [4] Davis, L., MacDonald, N., Palmberg, P., Riach, G. and Weber, R. (1972). *The Handbook of Auger Electron Spectroscopy*. 2nd ed. Eden Prairie: Physical Electronics Industries Inc.
- [5] Davis, L., MacDonald, N., Palmberg, P., Riach, G. and Weber, R. (1972). *Handbook of Photoelectron Spectroscopy*. 2nd ed. Eden Prairie: Physical Electronics Industries Inc.